JOURNAL OF APPLIED PHYSICS **121**, 244301 (2017)

Electric field distribution and current emission in a miniaturized geometrical diode

Jinpu Lin,[1] Patrick Y. Wong,[1] Penglu Yang,[2] Y. Y. Lau,[1] W. Tang,[3] and Peng Zhang[1,2,a)]
[1]*Department of Nuclear Engineering and Radiological Sciences, University of Michigan, Ann Arbor, Michigan 48109-2104, USA*
[2]*Department of Electrical and Computer Engineering, Michigan State University, East Lansing, Michigan 48824-1226, USA*
[3]*Directed Energy Directorate, Air Force Research Laboratory, Albuquerque, New Mexico 87117, USA*

(Received 31 March 2017; accepted 8 June 2017; published online 23 June 2017)

We study the electric field distribution and current emission in a miniaturized geometrical diode. Using Schwarz-Christoffel transformation, we calculate exactly the electric field inside a finite vacuum cathode-anode (A-K) gap with a single trapezoid protrusion on one of the electrode surfaces. It is found that there is a strong field enhancement on both electrodes near the protrusion, when the ratio of the A-K gap distance to the protrusion height $d/h < 2$. The calculations are spot checked against COMSOL simulations. We calculate the effective field enhancement factor for the field emission current, by integrating the local Fowler-Nordheim current density along the electrode surfaces. We systematically examine the electric field enhancement and the current rectification of the miniaturized geometrical diode for various geometric dimensions and applied electric fields. *Published by AIP Publishing.* [http://dx.doi.org/10.1063/1.4987127]

I. INTRODUCTION

There is a growing interest in the miniaturization of anode-cathode (A-K) gaps by using fine emission tips to realize a nanoscale diode.[1–12] The geometrically asymmetric metal-vacuum (insulator)-metal nanoscale diode shows great potential for applications in energy harvesting and energy conversion in solar cells,[13–15] as well as for high power high frequency applications in signal rectification and electron source development.[2,16–23] Bringing a sharp anode tip sufficiently close to the graphene surface has realized electron emission from flat graphene surfaces.[24] Thus, it is of value to assess the electrical field distribution and current emission inside the miniaturized A-K gap and their asymmetry introduced by the protruding surface of the electrode.

Electric field distribution on knife-edge field emitters was calculated using conformal mapping.[25,26] The method has later been extended to the studies of the electric field enhancement of several rectilinear geometries,[27,28] of the electric field screening by the proximity of two knife-edge field emitters,[29] and of asperity in a channel for microscale gas breakdown.[30] These existing models on field emitters usually assume that the emission tip is far away from the anode, whose effect on the tip field enhancement is thus ignored. However, the finite tip-anode distance is comparable to or even smaller than the tip height, as is often the case in experiments.[21,31,32] Recent studies[33,34] on the effects of finite A-K gap focus only on emitters with vertical walls, where the current rectification behaviors remains unexplored.

In this paper, we study the electric field distribution and field emission current in a *finite* A-K gap with a single trapezoidal protrusion (Fig. 1), which may represent a miniaturized geometrical vacuum diode. The electric field inside the A-K gap is calculated exactly using the Schwarz-Christoffel transformation.[26] From these exact electric field profiles, we calculate the effective field enhancement factor for the field emission current, where the flat electrode or the electrode with a protrusion can either be the cathode or anode, depending on the sign of bias. This allows our quantitative assessment of current rectification. Scaling of the fields and the current is studied as a function of geometry and bias voltage.

Section II presents the theoretical formulation. In Sec. III, results and discussion are given for various aspect ratios, geometries, and applied bias voltages. Section IV presents a summary and suggestions for future research.

II. FORMULATION

Consider an anode-cathode (A-K) geometry with a trapezoidal tip, as shown in Fig. 1(a). The A-K gap distance is d, the tip has half width a, height h, and angle with the substrate α. We solve the electric field inside the gap by conformal mapping between the complex $z-$ and $w-$ planes where $z = x + iy = (x, y)$ and $w = u + iv = [u, v]$. Following Ref. 25, we denote this mapping as $(x, y) \leftrightarrow [u, v]$ henceforth [Fig. 1(b)]. Specifically, the maps of $ABCDE_1E_2FG$ in Fig. 1 are, sequentially, $(\infty, d) \leftrightarrow [-\infty, 0]$, $(-\infty, d) \leftrightarrow [0^-, 0]$, $(-\infty, 0) \leftrightarrow [0^+, 0]$, $(-a - h\cot\alpha, 0) \leftrightarrow [1, 0]$, $(-a, h) \leftrightarrow [u_3, 0]$, $(a, h) \leftrightarrow [u_3', 0]$, $(a + h\cot\alpha, 0) \leftrightarrow [u_4, 0]$, and $(\infty, 0) \leftrightarrow [\infty, 0]$. In the maps B' and C', 0^+ and 0^- denote values slightly greater and less than zero, respectively. This map is governed by the Schwarz-Christoffel transformation[26]

$$z = K \int_{w_0}^{w} f(w')dw' + z_0, \tag{1}$$

a)Author to whom correspondence should be addressed: pz@egr.msu.edu

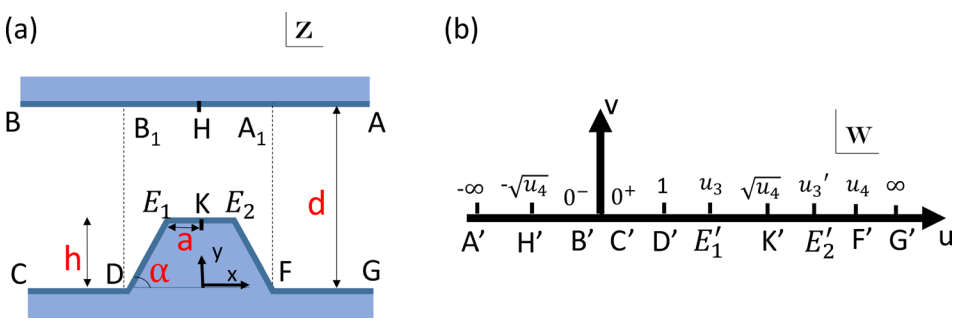

FIG. 1. (a) Anode-cathode (A-K) gap with a trapezoidal tip in the $z \equiv (x, y)$ plane and (b) its map onto the $w \equiv [u, v]$ plane.

$$f(w) = \frac{1}{w}\left(\frac{w-u_3}{w-1}\frac{w-u_3'}{w-u_4}\right)^{\alpha/\pi}, \tag{2}$$

where K, u_3, u_3', and u_4 are constants to be determined, and $z_0(x_0, y_0) \leftrightarrow w_0[u_0, v_0]$ is an arbitrary point along the boundary of $ABCDE_1E_2FG$ and the corresponding u-axis. Without loss of generality, we choose point D, that is $z_0 = -a - h\cot\alpha + i0$ and $w_0 = 1 + i0$ in Eq. (1). Branch cuts [not shown in Fig. 1(b)] extending downward from the branch points render $f(w)$ single valued in the upper half w-plane.

The complex electrostatic potential is $\Phi(w) = ikE_0 \log(w) = \phi + i\psi$. It represents a circulation electric field about the origin, which is the singularity point where points B' and C' coincide.[25,26,30] This potential is chosen so that both the negative u-axis and the positive u-axis are equipotential lines, which produce a constant uniform electric field $(-iE_0)$ far away from the protrusion (Fig. 1). To see this, the components E_x and E_y of the electrostatic field in the (x, y) plane may be expressed as[25,29]

$$E_x - iE_y = -\frac{d\Phi}{dz} = -\frac{d\Phi/dw}{dz/dw} = -iE_0\left(\frac{w-1}{w-u_3}\frac{w-u_4}{w-u_3'}\right)^{\alpha/\pi}, \tag{3}$$

where we have used Eqs. (1) and (2) for dz/dw. Equation (3) clearly shows a constant electric field $-iE_0$ at $w = \infty$. As $w \to 0$, the electric field becomes $E_x - iE_y = -iE_0(u_4/u_3u_3')^{\alpha/\pi}$, which should be the same as the field when $w = \infty$. Thus, this gives

$$u_4 = u_3u_3'. \tag{4}$$

Using Eqs. (1) and (4), it is easy to show that the maps for H and K (Fig. 1) are, respectively, $H(0, d) \leftrightarrow H'\left[-\sqrt{u_4}, 0\right]$ and $K(0, h) \leftrightarrow K'\left[\sqrt{u_4}, 0\right]$. Evaluating $z(w)$ at points B and C and subtracting the two obtained equations, we have

$$K = \frac{d}{\pi}, \tag{5}$$

where we have used Eq. (4). Evaluating $z(w)$ at points E_1 and E_2, we obtain, respectively,

$$\frac{\pi}{\sin\alpha}\frac{h}{d} = \int_1^{u_3}\frac{1}{u}\left(\frac{u_3-u}{u-1}\frac{u_3'-u}{u_3u_3'-u}\right)^{\alpha/\pi}du, \tag{6}$$

$$2\pi\frac{a}{d} = \int_{u_3}^{u_3'}\frac{1}{u}\left(\frac{u-u_3}{u-1}\frac{u_3'-u}{u_3u_3'-u}\right)^{\alpha/\pi}du, \tag{7}$$

where we have used Eq. (5). For any given values of angle α and aspect ratios a/d and h/d, the unknown variables u_3 and u_3' can be solved from Eqs. (6) and (7) numerically, and u_4 follows from Eq. (4). The electric field everywhere inside the A-K gap in Fig. 1(a) is then calculated from Eq. (3). The local electric field enhancement is defined as

$$\beta = \left|\frac{E}{E_0}\right| = \frac{\sqrt{E_x^2 + E_y^2}}{E_0}, \tag{8}$$

where E_0 is the uniform electric field far away from the trapezoidal tip.

For field emission, the current density is obtained from the Fowler-Nordheim (FN) equation[35]

$$J = A_{FN}E_c^2\exp\left(-\frac{B_{FN}}{E_c}\right)\left[\frac{\mathrm{A}}{\mathrm{m}^2}\right], \tag{9}$$

where $A_{FN} = \frac{1.5\times10^{-6}}{W}\exp\left(\frac{10.4}{\sqrt{W}}\right)$, $B_{FN} = 6.44\times10^9W^{3/2}$, E_c is the local cathode electric field in V/m, and W is the work function of the cathode in eV. When the electrode with the trapezoidal tip is the cathode, the average current density from the tip may then be calculated based on Eq. (9) as

$$J_{avg1} = \frac{A_{FN}\int_{DE_1E_2F}E_C^2(s)\exp\left(-\frac{B_{FN}}{E_c(s)}\right)ds}{DF}, \tag{10}$$

where the line integral is taken along the path DE_1E_2F, $E_c(s)$ is the local electric field at the point s along the path, and $DF = 2a + 2hcot(\alpha)$ is the length between points D and F [Fig. 1(a)]. Likewise, when the flat electrode is the cathode, the average current density emitted is calculated as

$$J_{avg2} = \frac{A_{FN}\int_{A_1B_1}E_C^2(s)\exp\left(-\frac{B_{FN}}{E_c(s)}\right)ds}{A_1B_1}, \tag{11}$$

where $E_c(s)$ is now the local electric field at the point s along the path A_1B_1, with the length $A_1B_1 = DF$ [Fig. 1(a)].

From the averaged current density in Eqs. (10) and (11), one may obtain the effective field enhancement factor $\beta_{eff1,2}$ from

$$J_{avg1,2} = A_{FN}\beta_{eff1,2}^2E_0^2\exp\left(-\frac{B_{FN}}{\beta_{eff1,2}E_0}\right), \tag{12}$$

where $E_0 = V_g/d$, with V_g and d being the applied gap voltage and the A-K gap distance, respectively. Note that the

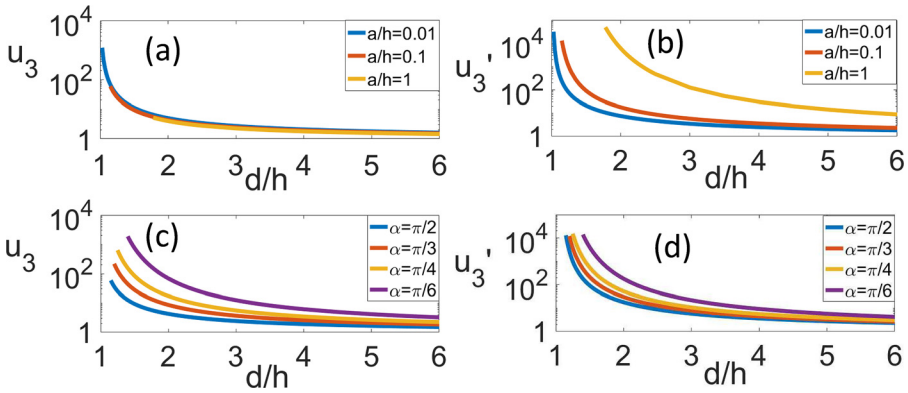

FIG. 2. (a) u_3 and (b) u_3' as a function of d/h for various a/h when $\alpha = \pi/2$ and (c) u_3 and (d) u_3' as a function of d/h for different α values when $a/h = 0.1$.

effective electric field enhancement factor in Eq. (12) is a function of the applied electric field E_0, whereas the local field enhancement factor in Eq. (8) is independent of E_0. The effective field enhancement has been studied in numerous previous works.[28,36–38]

III. RESULTS AND DISCUSSION

Figure 2 shows the values of u_3 and u_3' [c.f. Fig. 1(b)] as a function of the ratio of gap separation to tip height d/h for different values of the tip aspect ratio a/h and angle α. It is clear that u_3 and u_3' become very sensitive to d/h when $d/h < 5$, indicating a strong effect of the finite gap distance on the electric field distribution in this regime.

Figure 3 plots the local electric field enhancement factor $\beta = |E/E_0|$ along the two electrode surfaces, AB, and CDE_1E_2FG, and along the symmetric axis KH in Fig. 1(a), calculated from Eq. (8). Note that the fields along the two electrode surfaces are plotted against the position on the x-axis normalized to h, real(z/h), and those along the symmetric axis are against the position on the y-axis normalized to d, imag(z/d). Field enhancement is found at both the flat and protrusive electrodes, with a strong dependence on d/h. As d/h increases, the local field enhancement factor at both the flat and protrusive surfaces decreases, as shown in Figs. 3(a)–3(c). The effects of a/h on the field enhancements are shown in Figs. 3(d)–3(f). As a/h increases, the local field enhancement at the flat surface increases; this is because more surface area of the flat electrode becomes closer to the other electrode, thus leading to a smaller effective A-K gap. However, the local field enhancement at the protrusive surface (i.e., the tip) decreases as a/h increases, since the sharpness of the tip decreases with increasing a/h. The dependence of the field enhancements on the angle α is shown in Figs. 3(g)–3(i). As α increases, the average distance between the tip and the flat electrode [DF to B_1A_1 in Fig. 1(a)] decreases, leading to a reduction on the field enhancement on the flat electrode. However, as the sharpness of the tip increases with α, the field enhancement on the tip is increased. In Figs. 3(c), 3(f), and 3(i), electric field profiles along the symmetric axis KH obtained from COMSOL[39] simulation are also shown. Excellent agreement between conformal mapping and the numerical simulation is obtained.

Figure 4 shows the local field enhancement factor at the center points of the two electrodes K and H [c.f. Fig. 1(a)] as a function of the ratio of gap separation to tip height d/h for different values of the tip aspect ratio a/h and angle α. Field enhancements at both the flat and protrusive electrodes

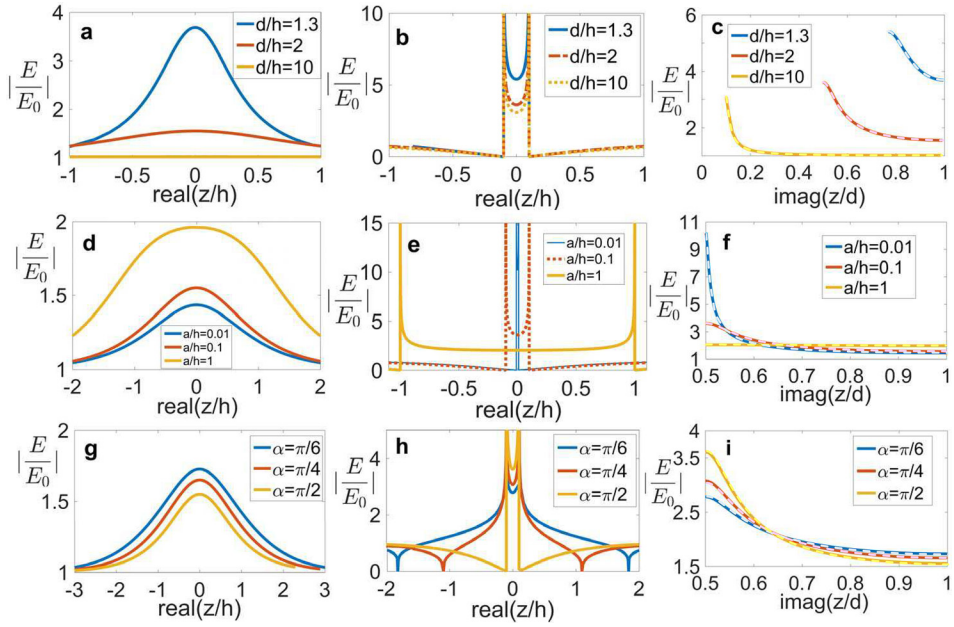

FIG. 3. The normalized electric field [i.e., local electric field enhancement factor β from Eq. (8)] against normalized position for (a)–(c) $d/h = 1.3$, 2, and 10 with $a/h = 0.1$ and $\alpha = \pi/2$, (d)–(f) $a/h = 0.01$, 0.1, and 1 with $d/h = 2$ and $\alpha = \pi/2$, (g)–(i) $\alpha = \pi/6$, $\pi/4$, and $\pi/2$ with $d/h = 2$ and $a/h = 0.1$. (a), (d), and (g) are along the flat electrode surface AB; (b), (e), and (h) are along the protrusive electrode surface CDE_1E_2FG, plotted against the position on the x-axis (normalized to h); and (c), (f), and (i) are along the symmetric axis KH. Dashed lines in (c), (f), and (i) are from COMSOL simulations.

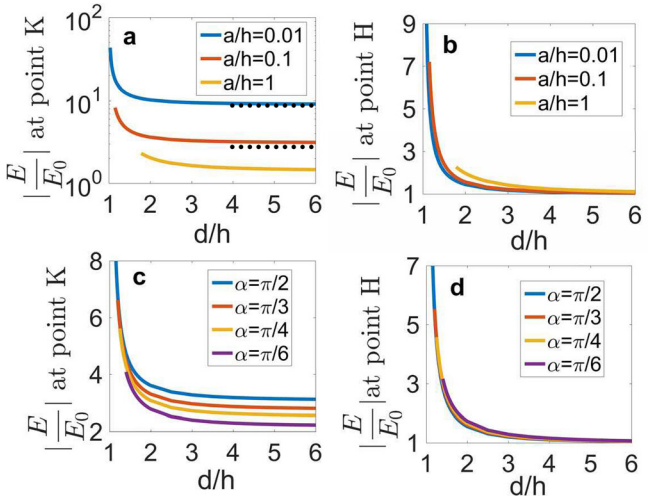

FIG. 4. Local electric field enhancement factor $\beta = |E/E_0|$ calculated from Eq. (8) at the center of the two electrodes (a) point K and (b) point H as a function of d/h for various a/h values when $\alpha = \pi/2$; and at (c) point K and (d) point H as a function of d/h for different α values when $a/h = 0.1$. Dotted lines in (a) are for $|E/E_0| = \sqrt{\pi h/4a}$ when $a/h \ll 1$, which is the result obtained by assuming d approaches infinity.[25]

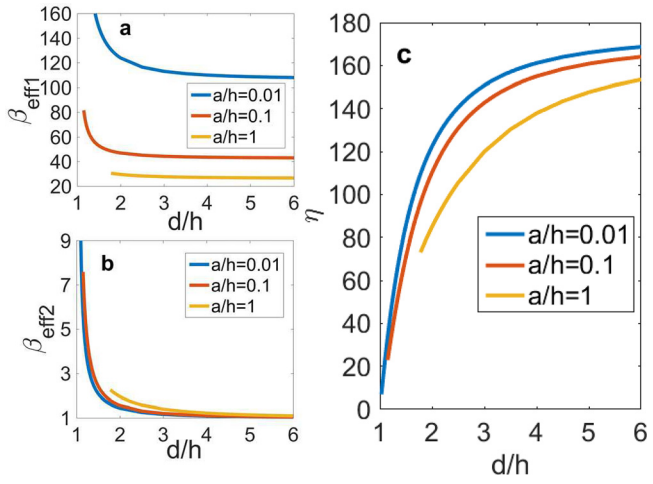

FIG. 5. The effective field enhancement factor calculated from Eq. (12) at (a) the protrusive electrode surface DE_1E_2F, (b) the flat electrode surface A_1B_1, and (c) the corresponding current rectification ratio, $\eta = J_{avg1}/J_{avg2}$, as a function of d/h, for $a/h = 0.01$, 0.1, and 1, with $\alpha = \pi/2$. In the calculation, it is assumed that the uniform electric field far from the tip $E_0 = 3 \times 10^8$ V/m, and the work function of both electrodes $W = 4$ eV.

increase rapidly as d/h decreases, for $d/h < 2$. When $d/h > 5$, the field enhancement at the center of the flat surface point H converges to the constant value of 1, and those at tip center point K approach almost constant values greater than 1. As shown in Fig. 4(a), for the special cases of $\alpha = \pi/2$, these constant values agree well with $\sqrt{\pi h/4a}$ when $a/h \ll 1$, which is obtained by assuming that d approaches infinity.[25] The field enhancement at the tip center is also strongly dependent on a/h and α, whereas that at the center of the flat electrode is insensitive to a/h and α. The results are consistent with those shown in Fig. 3.

For field emission current in the geometric diode, the effective field enhancement factors on both the protrusion surface (DE_1E_2F) β_{eff1} and the flat surface (A_1B_1) β_{eff2} are plotted in Figs. 5(a) and 5(b), as a function of d/h for $a/h = 0.01$, 0.1, and 1, with $\alpha = \pi/2$. In the calculation, we assume that the uniform electric field far from the tip is $E_0 = 3 \times 10^8$ V/m and the work function of the electrodes $W = 4$ eV. It can be seen that the effective field enhancement factors on both surfaces $\beta_{eff1,2}$ increase significantly when d/h decreases, for d/h less than 2. $\beta_{eff1,2}$ approaches almost constant values when $d/h > 5$. The parametric dependence of the effective field enhancement and those of the local field enhancement (Fig. 4) are very similar. The emission current rectification ratio, $\eta = J_{avg1}/J_{avg2}$, is shown in Fig. 5(c), where J_{avg1} and J_{avg2} are calculated from Eqs. (10) and (11), respectively. It is seen that η increases as d/h increases or a/h decreases. As the A-K gap distance decreases in the miniaturized diode, e.g., $d/h < 2$, the current rectification ratio η drops significantly. The theoretical analysis of the current rectification η here would provide insights into the design of geometric diode with optimal rectification efficiency for various applications.[13–23]

Figures 6(a) and 6(b) show the effective field enhancement factors $\beta_{eff1,2}$ as a function of a/h for $d/h = 1.3$, 2, and 10, with $\alpha = \pi/2$. For a given d/h, as a/h increases, β_{eff1} decreases, while β_{eff2} increases. This is expected since as a/h increases, the sharpness of the tip decreases, thus leading to a smaller field enhancement factor at the protrusive electrode. On the other hand, the effective A-K gap distance decreases as the tip width a increases, thus giving a larger β_{eff2} on the flat surface. The emission current rectification ratio, $\eta = J_{avg1}/J_{avg2}$, is shown in Fig. 6(c). In general, η decreases as a/h increases. The aspect ratio of the tip a/h has a stronger effect on $\beta_{eff1,2}$ and η when the effective gap distance d/h becomes smaller. It is important to point out that the Fowler-Nordheim equation [Eq. (9)] is only valid when the Schottky barrier reduction is small compared to the work function, $\sqrt{e^3E/4\pi\epsilon_0} < W$. To the lowest order, this requires that the local Schottky barrier reduction at the tip center [point K in Fig. 1(a)] to be smaller than the work function there, which gives the lower limit of $a/h > \left(\frac{1}{64\pi}\right)\left(\frac{eE_0[V/m]}{\epsilon_0(W[eV])^2}\right)^2$, for which

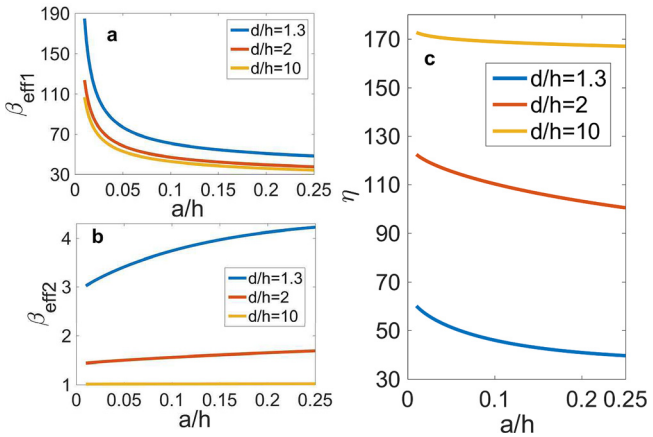

FIG. 6. The effective field enhancement factor at (a) the protrusive electrode surface DE_1E_2F and (b) the flat electrode surface A_1B_1, and (c) the current rectification ratio, as a function of a/h, calculated from Eqs. (10)–(12), for $d/h = 1.3$, 2, and 10, with $\alpha = \pi/2$, $E_0 = 3 \times 10^8$ V/m, and work function $W = 4$ eV.

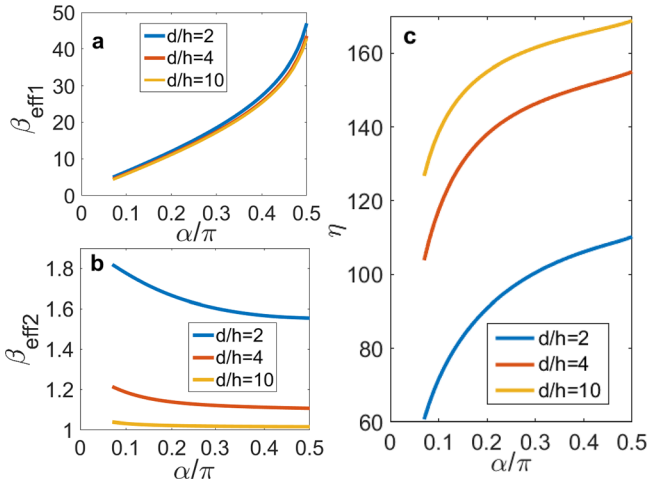

FIG. 7. The effective field enhancement factor at (a) the protrusive electrode surface DE_1E_2F and (b) the flat electrode surface A_1B_1, and (c) the current rectification ratio, as a function of α, calculated from Eqs. (10)–(12), for $d/h = 2$, 4, and 10, with $a/h = 0.1$, $E_0 = 3 \times 10^8$ V/m, and work function $W = 4$ eV.

the effective field enhancement factor β_{eff} may be representative of possible real wedge-geometries. In deriving this limit, we have used the local (not effective) field enhancement at the center of the tip $\beta = |E/E_0| = \sqrt{\pi h/4a}$ for a vertical emitter when $a/h \ll 1$ (c.f. Fig. 4 and Ref. 25). For the parameters used in Fig. 6 (and other figures), this lower limit gives $a/h > 5.72 \times 10^{-4}$, well below the range of a/h used in our calculation.

The effects of angle α on $\beta_{eff1,2}$ and η are shown in Fig. 7. As α increases, β_{eff1} increases rapidly, while β_{eff2} decreases only slightly. This is because the sharpness of the tip is effectively increased as α increases, and therefore, the effective field enhancement factor increases for the tip. However, the effective gap distance between the protrusive and the flat surfaces increases and the effective emission area (A_1B_1) decreases when α increases, which induces a slight decrease in β_{eff2}. The emission current rectification ratio, $\eta = J_{avg1}/J_{avg2}$, is shown in Fig. 7(c). For a given d/h and a/h, η increases as α increases.

Figure 8 shows the effects of the applied electric field E_0 on $\beta_{eff1,2}$ and η. As E_0 increases, larger surface area (with a relatively low local field enhancement factor) near the tip would be able to emit current, and thus, the effective field enhancement β_{eff1} would decrease on average. On the flat electrode, β_{eff2} is insensitive to E_0. The emission current rectification ratio, $\eta = J_{avg1}/J_{avg2}$, decreases significantly as E_0 increases when $E_0 < 2 \times 10^8$ V/m, as shown in Fig. 8(c).

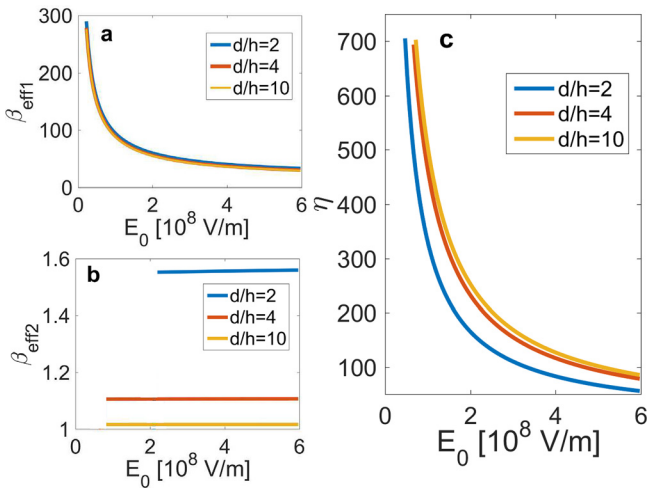

FIG. 8. The effective field enhancement factor at (a) the protrusive electrode surface DE_1E_2F and (b) the flat electrode surface A_1B_1, and (c) the current rectification ratio, as a function of E_0, calculated from Eqs. (10)–(12), for $d/h = 2$, 4, and 10, with $a/h = 0.1$, $\alpha = \pi/2$, and work function $W = 4$ eV.

IV. CONCLUSIONS

We have systematically studied the electric field distribution and field emission current in a miniaturized geometrical diode, consisting of a finite A-K gap with a single trapezoidal protrusion. The electric field inside the A-K gap and the local field enhancement are calculated exactly using the Schwarz-Christoffel transformation. The calculation is spot-checked using COMSOL. Limiting cases are recovered when the A-K gap distance becomes large compared to the protrusion height. It is found that there is strong field enhancement on both electrodes near the protrusion as the A-K gap decreases to be comparable with the protrusion height. The effective field enhancement factor and the current rectification ratio of the diode are calculated for field emission current, by using the Fowler-Nordheim (FN) equation for the current density. Scaling of the fields and the current is studied as a function of various geometric ratios and the biased electric fields. The scaling of the current rectification ratio would provide guidance in optimizing the design of miniaturized geometric diodes for various high power high frequency applications.

It is worth noting that the FN law is derived by assuming only a single emitting surface without the effects of the other electrode. Although previous studies suggest that the FN law is accurate at the intermediate voltage level in a nanoscale AK gap,[40,41] our FN based approach here should be viewed only as a first approximation. A more accurate approach is to convert the field distribution into the potential profile and solve the current transmission directly from the Schrodinger equation.[15]

Further research may consider the effects of quantum tunneling for current emission when the A-K gap distance is decreased to nanometer scale,[12,40,41] AC response of the diode under high frequency excitation,[15,42,43] electric field screening effect for an array of emission tips,[2,29] possible new emission physics such as inverse tunneling,[44] and experimental validation of the theory.

ACKNOWLEDGMENTS

This work was supported by AFOSR Grant No. FA9550–14-0309. P. Yang and P. Zhang were also supported by AFOSR through a subcontract from the University of Michigan.

[1]F. Yesilkoy, S. Potbhare, N. Kratzmeier, A. Akturk, N. Goldsman, M. Peckerar, and M. Dagenais, in *Rectenna Solar Cells*, edited by G. Moddel and S. Grover (Springer, New York, 2013), pp. 163–188.
[2]N. M. Miskovsky, P. H. Cutler, A. Mayer, B. L. Weiss, B. Willis, T. E. Sullivan, and P. B. Lerner, J. Nanotechnol. **2012**, e512379.

[3]K. Choi, G. Ryu, F. Yesilkoy, A. Chryssis, N. Goldsman, M. Dagenais, and M. Peckerar, J. Vac. Sci. Technol. B **28**, C6O50 (2010).
[4]J.-W. Han, J. S. Oh, and M. Meyyappan, Appl. Phys. Lett. **100**, 213505 (2012).
[5]J.-W. H. M. Meyyappan, see http://spectrum.ieee.org/semiconductors/devices/introducing-the-vacuumtransistor-a-device-made-of-nothing for Introducing the Vacuum Transistor: A Device Made of Nothing, 23 June 2014.
[6]S. Srisonphan, Y. S. Jung, and H. K. Kim, Nat. Nanotechnol. **7**, 504 (2012).
[7]J. Xu, Q. Wang, Z. Qi, Y. Zhai, and X. Zhang, J. Appl. Phys. **117**, 204504 (2015).
[8]Y. B. Zhu, P. Zhang, A. Valfells, L. K. Ang, and Y. Y. Lau, Phys. Rev. Lett. **110**, 265007 (2013).
[9]P. Zhang and D. M. H. Hung, J. Appl. Phys. **115**, 204908 (2014).
[10]P. Zhang and Y. Y. Lau, J. Plasma Phys. **82**, 595820505 (2016).
[11]F. Antoulinakis, D. Chernin, P. Zhang, and Y. Y. Lau, J. Appl. Phys. **120**, 135105 (2016).
[12]P. Zhang, A. Valfells, L. K. Ang, J. W. Luginsland, and Y. Y. Lau, Appl. Phys. Rev. **4**, 011304 (2017).
[13]*Rectenna Solar Cells*, 2013 ed., edited by G. Moddel and S. Grover (Springer, New York, 2013).
[14]N. M. Miskovsky, S. J. Shepherd, P. H. Cutler, T. E. Sullivan, and A. A. Lucas, Appl. Phys. Lett. **35**, 560 (1979).
[15]A. Mayer, M. S. Chung, B. L. Weiss, N. M. Miskovsky, and P. H. Cutler, Phys. Rev. B **77**, 085411 (2008).
[16]A. Evtukh, H. Hartnagel, O. Yilmazoglu, H. Mimura, and D. Pavlidis, *Vacuum Nanoelectronic Devices: Novel Electron Sources and Applications*, 1st ed. (Wiley, Chichester, West Sussex, United Kingdom, 2015).
[17]K. L. Jensen, Phys. Plasmas **6**, 2241 (1999).
[18]K. L. Jensen, *Wiley Encyclopedia of Electrical and Electronics Engineering* (Wiley, 2014), Vol. 1.
[19]J. H. Booske, Phys. Plasmas **15**, 055502 (2008).
[20]D. Shiffler, T. K. Statum, T. W. Hussey, O. Zhou, and P. Mardahl, in *Modern Microwave and Millimeter-Wave Power Electronics* (IEEE, Piscataway, NJ, 2005), p. 691.
[21]W. Tang, D. Shiffler, K. Golby, M. LaCour, and T. Knowles, J. Vac. Sci. Technol. B **30**, 061803 (2012).
[22]W. Tang, D. Shiffler, K. Golby, M. LaCour, and T. Knowles, J. Vac. Sci. Technol. B: Nanotechnol. Microelectron. Mater. Process. Meas. Phenom. **32**, 052202 (2014).
[23]J. R. Harris, K. L. Jensen, and D. A. Shiffler, J. Appl. Phys. **119**, 043301 (2016).
[24]S. Santandrea, F. Giubileo, V. Grossi, S. Santucci, M. Passacantando, T. Schroeder, G. Lupina, and A. D. Bartolomeo, Appl. Phys. Lett. **98**, 163109 (2011).
[25]R. Miller, Y. Y. Lau, and J. H. Booske, Appl. Phys. Lett. **91**, 074105 (2007).
[26]F. B. Hildebrand, *Advanced Calculus for Applications*, 1st ed. (Prentice Hall Inc., Englewood Cliffs, New Jersey, 1962).
[27]R. Miller, Y. Y. Lau, and J. H. Booske, J. Appl. Phys. **106**, 104903 (2009).
[28]R. Miller, "Investigations of geometric field enhancement and electron field emission using conformal mapping," Ph.D. dissertation (University of Wisconsin, 2009).
[29]W. Tang, D. Shiffler, and K. L. Cartwright, J. Appl. Phys. **110**, 034905 (2011).
[30]A. Venkattraman, J. Phys. Appl. Phys. **47**, 425205 (2014).
[31]K. Asaka, H. Nakahara, and Y. Saito, Appl. Phys. Lett. **92**, 023114 (2008).
[32]H. S. Sim, S. P. Lau, L. K. Ang, G. F. You, M. Tanemura, K. Yamaguchi, M. Zamri, and M. Yusop, Appl. Phys. Lett. **93**, 023131 (2008).
[33]X.-Z. Qin, W.-L. Wang, N.-S. Xu, Z.-B. Li, and R. G. Forbes, Proc. R. Soc. London Math. Phys. Eng. Sci. **467**, 1029 (2010).
[34]X. Qin, W. Wang, and Z. Li, J. Vac. Sci. Technol. B: Nanotechnol. Microelectron. Mater. Process. Meas. Phenom. **29**, 031802 (2011).
[35]R. H. Fowler and L. Nordheim, Proc. R. Soc. London Ser. A **119**, 173 (1928).
[36]Y. Feng and J. P. Verboncoeur, Phys. Plasmas **12**, 103301 (2005).
[37]K. L. Jensen, J. Appl. Phys. **107**, 014905 (2010).
[38]K. L. Jensen, J. Lebowitz, Y. Y. Lau, and J. Luginsland, J. Appl. Phys. **111**, 054917 (2012).
[39]See https://www.comsol.com/ for the COMSOL Multiphysics® Modeling Software.
[40]P. Zhang, Sci. Rep. **5**, 9826 (2015).
[41]J. G. Simmons, J. Appl. Phys. **34**, 1793 (1963).
[42]P. Zhang and Y. Y. Lau, Sci. Rep. **6**, 19894 (2016).
[43]K. Yoshioka, I. Katayama, Y. Minami, M. Kitajima, S. Yoshida, H. Shigekawa, and J. Takeda, Nat. Photonics **10**, 762 (2016).
[44]P. Zhang and T. Pan, AIP Adv. **7**, 065307 (2017).